

DETECTABILITY IN THE PRESENCE OF COMPUTED TOMOGRAPHIC RECONSTRUCTION NOISE*

Kenneth M. Hanson
University of California, Los Alamos Scientific Laboratory
Los Alamos, New Mexico 87545

Abstract

If the standard filtered backprojection algorithm with a filter of the form $g(f) = |f|h(f)$ is applied to noisy projections, all of which have a noise power spectral density (NPSD), $S_{\text{proj}}(f)$, then the resulting computed tomographic (CT) reconstruction has a two dimensional NPSD of the form, $S(f) \sim |f||h(f)|^2 S_{\text{proj}}(f)$. For proper reconstruction, $h(f)$ must approach a non-zero constant as $f \rightarrow 0$. Provided $S_{\text{proj}}(f)$ is constant, i.e. white projection noise, the CT noise at low frequencies is suppressed by the $|f|$ factor. This low frequency suppression results in a long range negative spatial correlation of the CT noise. If white noise is spatially averaged over a circle of diameter d , then the variance in the averaged values will behave as $\sigma^2 \sim d^{-2}$. For CT noise the variance drops faster than d^{-2} . Simple signal-to-noise ratio considerations suggest that the dependence of minimum detectable contrast upon the diameter of the circle to be detected could be significantly different in the presence of CT noise than in that of white noise. Simulated reconstructions of a suitable detectability pattern demonstrate these differences may not exist unless the image is spatially smoothed before observation. It is pointed out that the pixel width used in the image display should be from 1/3 to 1/2 the width of the point spread function in order to avoid discrete binning problems.

Introduction

The multitude of commercial computed tomographic (CT) scanners which have recently been introduced for use in diagnostic radiology has given rise to a need to compare these different machines in terms of image quality and dose to the patient. It is therefore desirable to arrive at a figure of merit for a CT image which gives a measure of the diagnostic efficacy of that image. This figure of merit may well be dependent upon the specific visual task being performed. It is clearly important that the capabilities and deficiencies of the human observer as well as the interface between man and machine, namely the viewing system, be taken into account in formulating the figure of merit. Since the CT reconstruction is the result of computer processing, it is possible to use this processing to alter the characteristics of the displayed images. This image processing may improve or degrade the figure of merit.

It has been pointed out by Riederer, Pelc and Chesler⁽¹⁾ that if projection data containing uncorrelated noise are used to perform a CT reconstruction, the noise in the reconstructed image possesses unusual correlations not found in ordinary radiographs. It is the purpose of this paper to explore the effects that these correlations in ideal CT noise have upon the performance of a simple visual task, namely the detection of circles of varying size and contrast. If actual CT scanners produce images with similar noise characteristics, the results presented here may aid in the specification of a figure of merit for CT images in conjunction with this specific visual task.

1. Noise Power Spectra CT Noise

The noise in an image may be characterized by its power spectral density S , or alternatively by its autocorrelation function, which is the Fourier transform of S . A brief derivation of the noise power spectral density of CT reconstructions obtained by the filtered backprojection algorithm follows. We will use an approach and nomenclature similar to that used by Riederer, Pelc and Chesler⁽¹⁾. S is defined as the mean square amplitude of the Fourier transform of the image per unit area,

$$S(f_x, f_y) = \frac{1}{A} \left\langle \left| \iint_A dx dy r(x, y) e^{-2\pi i(xf_x + yf_y)} \right|^2 \right\rangle \quad (1)$$

where $r(x, y)$ is the reconstruction image containing only noise and the brackets indicate the ensemble average over all images obtained under identical conditions.

*The work presented here was performed under funding by the U.S. Energy Research and Development Administration.

DETECTABILITY IN THE PRESENCE OF COMPUTED TOMOGRAPHIC RECONSTRUCTION NOISE

It will be assumed that all projections have the same one dimensional noise power spectrum $S_p(f_x)$, and that the projections themselves are statistically independent. For projections containing band-limited white noise,

$$S_p(f) = \begin{cases} w \sigma_p^2, & |f| \leq f_N \\ 0, & |f| > f_N \end{cases}$$

where w is the bin width in the projection sampling, f_N is the Nyquist frequency, $f_N = (2w)^{-1}$, and σ_p^2 is the variance in the projection measurements. The normalization is such that the total power is

$$\sigma_p^2 = \int_{-f_N}^{f_N} df S_p(f) \tag{2}$$

The filter used in the reconstruction is of the form,

$$g(f) = |f|h(f). \tag{3}$$

For proper normalization of the reconstruction $h(f)$ approaches unity as f nears zero. The noise power spectrum of the filtered projection is

$$S_f(f) = |f|^2 |h(f)|^2 S_p(f). \tag{4}$$

When a single filtered projection is backprojected across the image in, say, the y direction, the resulting image does not vary with y . This leads to a δ -function in f_y when $S(f_x, f_y)$, Eq. 1, is calculated for one projection. The f_x dependence of S is the same as for the projection

$$S^{(1)}(f_x, f_y) \sim |f_x|^2 |h(f_x)|^2 S_p(f_x) \delta(f_y) \text{ (1 projection)}. \tag{5}$$

Figure 1a shows the contribution to the two dimensional noise power spectrum of one projection containing white noise for $h(f) = 1$. The δ -function is broadened due to the finite width of the reconstruction region. $S^{(1)}$ is merely a parabola along the spoke containing the f_x axis.

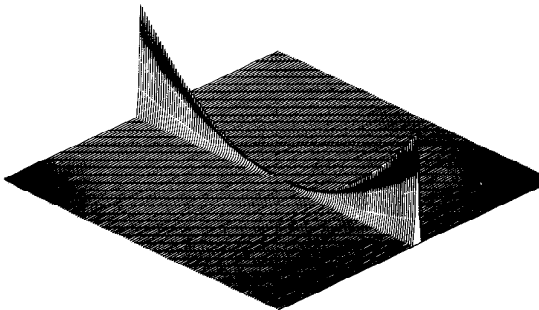


Figure 1a

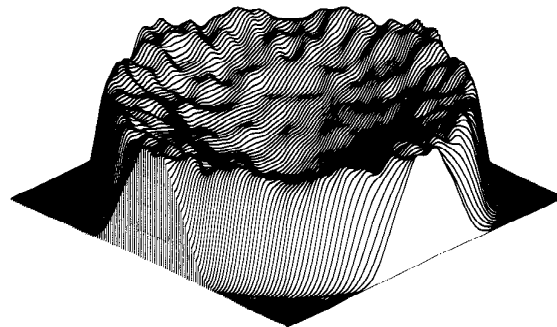


Figure 1b

Noise power spectral density distributions in two dimensional frequency space; (a) for a single input projection at 0° and (b) for a complete reconstruction from 300 projections.

HANSON

Let us consider what happens when m projections taken at equally spaced angles are included in the reconstruction. If the projections are statistically independent, it can be seen from Eq. 1 that S for the full reconstruction is simply the sum of $S^{(1)}$ for all projections. Since $S^{(1)}$ for the projection taken at an angle θ to the x -axis lies along a spoke through $f = 0$ at an angle θ to the f_x -axis, S is the sum of m such spokes. The result for S , with the proper normalization is

$$\begin{aligned}
 S(f) &= \frac{m}{f\pi} \left(\frac{\pi}{m}\right)^2 |f|^2 |h(f)|^2 S_p(f) \\
 &= \frac{\pi}{m} f |h(f)|^2 S_p(f)
 \end{aligned}
 \tag{6}$$

where $\frac{m}{f\pi}$ is the spoke density at the radial frequency f and $\frac{\pi}{m}$ arises from the normalization factor for the filtered backprojection algorithm.

In order to demonstrate that Equation 6 indeed gives the proper form, the noise power spectrum was calculated for a simulated noisy reconstruction. The 256×256 image was reconstructed from 300 projections, each containing 256 bins. The projection data consisted of Gaussian distributed white noise. The pure ramp filter ($h(f) = 1$) was used in the reconstruction procedure. S was estimated using the two dimensional extension of the method given by Welch.⁽²⁾ One observes in Fig. 1b that the resulting two dimensional noise power spectrum starts at a low value at zero frequency (center of plane), gradually increases up to the Nyquist frequency f_N (edges of plane) and finally falls off to zero beyond f_N . Figure 2 shows the average radial dependence of the estimate of $S(f)$ for two reconstruction filters. The dashed lines are the predictions based on Equation 6. The wiggles in the power spectra arise from the finite amount of data included in the estimate. The power estimate procedure involves averaging over portions of frequency space in order to reduce these wiggles. As a consequence, the power spectra in the region near zero frequency are filled in and the power spectra fall off before the Nyquist frequency.

The noise variance in the CT reconstruction may be found using Equation 6,

$$\begin{aligned}
 \sigma^2 &= \iint_{-\infty}^{\infty} df_x df_y S(f_x, f_y) \\
 &= \frac{\pi}{m} \int_0^{2\pi} d\phi \int_0^{f_N} df f^2 |h(f)|^2 S_p(f)
 \end{aligned}
 \tag{7}$$

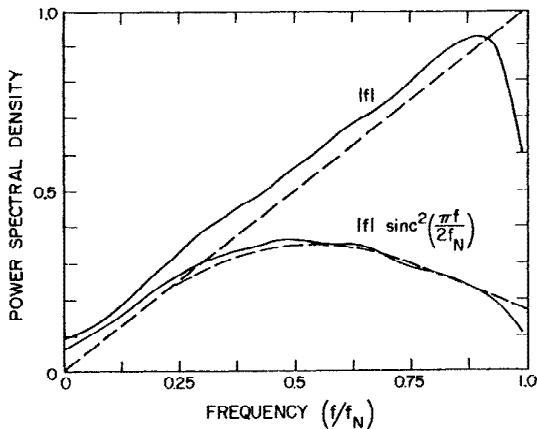


Figure 2

The dependence of the noise power spectral density upon $|f|$ shown with the solid curves for two choices of the projection filter function $g(f)$. The dashed lines show the expected dependence given by Equation 6.

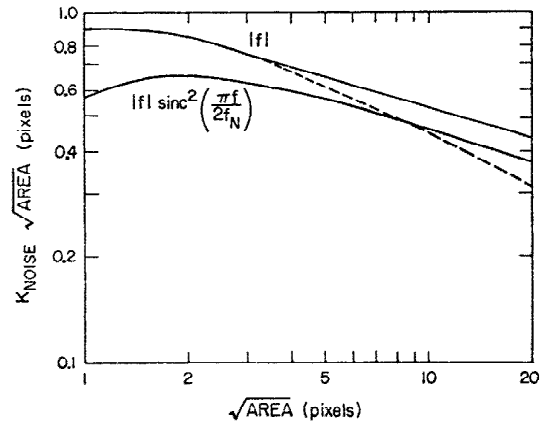


Figure 3

The solid curves show the relationship between the r.m.s. noise in CT reconstructions and the area for square averaging regions for two projection filter functions $g(f)$. The dashed curve indicates the effect of using a pyramidal averaging function for the ramp filter.

DETECTABILITY IN THE PRESENCE OF COMPUTED TOMOGRAPHIC RECONSTRUCTION NOISE

If the projection noise is white, this becomes

$$\sigma^2 = \frac{\sigma_p^2}{m^2 w^2} K_{\text{noise}}^2 \quad (8)$$

where

$$K_{\text{noise}}^2 = \frac{\pi^2}{4f_N^3} \int_0^{f_N} df \cdot f^2 |h(f)|^2 \quad (9)$$

It is assumed that the pixel width in the reconstruction is the same as the bin width in the projection w . K_{noise} as defined by Equation 8 provides a convenient means of comparing the noise propagation characteristics of different reconstruction algorithms. For the filtered backprojection algorithm, K_{noise} depends solely on $h(f)$. For $h = 1$, $K_{\text{noise}} = \frac{\pi}{\sqrt{12}} = 0.907$. For $h = \text{sinc}^2(\frac{\pi f}{2f_N})$, $K_{\text{noise}} = 0.568$.

2. Spatial Averaging

The effect of spatial averaging on the reconstructed image may be readily included in the foregoing formulism. Spatial averaging is essentially obtained by performing a convolution of the image with the averaging function. Convolution in real space is equivalent to filtering in frequency space, where the effective filter is the Fourier transform of the convolution function. Since the power spectral density is altered by the square of the applied filter, the noise variance is given by

$$\sigma^2 = \iint_{-\infty}^{\infty} df_x df_y S(f_x, f_y) |H(f_x, f_y)|^2 \quad (10)$$

where H is the effective filter applied to the reconstructed image. Maintaining the definition of K_{noise} , we have

$$K_{\text{noise}}^2 = \frac{\pi}{8f_N^3} \iint_{-\infty}^{\infty} df_x df_y |f| |h(f)|^2 |H(f_x, f_y)|^2 \quad (11)$$

where the integration is over the circle bounded by the Nyquist frequency f_N . Caution must be exercised when computing H since the spatial averaging is done with a finite number of pixel elements. Hence, H must be obtained by using the two dimensional discrete rather than the continuous Fourier transform of the averaging function.

Figure 3 shows the effect of averaging over square regions on the r.m.s. noise for two reconstruction filters. These curves were obtained by performing the averaging on the stimulated 256×256 reconstructions described above, instead of using the foregoing formulism. For circular averaging areas, very similar results are obtained. The data in Fig. 3 are presented in such a way that white noise would produce a horizontal straight line on such a plot. The slope of the two solid lines is approximately -0.30 for $\sqrt{\text{AREA}}$ greater than 4 pixels. From Equation 11 it can be seen that for $h = 1$, $K_{\text{noise}}^2 \sim (\text{AREA})^{-3/2}$ if H fell off somewhat faster than f^2 . Then the slope in Fig. 3 would be $-1/2$. The failure of the square averaging to produce this slope arises from the weak falloff of the corresponding H . The dashed line in Fig. 3 shows the effect of using a pyramidal weighting function. Its slope above 5 pixels, -0.50 , is as predicted since the corresponding H falls off faster than that for square averaging. In the latter example, the area of averaging is defined as the ratio of the variance of the unfiltered image to the variance of the filtered image for an image containing only white noise.

Riederer, Pelc and Chesler⁽¹⁾ have already noted that for CT reconstructions the r.m.s. noise is reduced faster when averaging is performed over square regions than when it is performed over thin rectangular regions of the same area. From Fig. 3 we observe further that the details of the weighting used in averaging over a square or circular region influence the magnitude of the noise reduction.

It should be pointed out that the images displayed by commercial CT scanners may not have precisely the same noise characteristics as described above. Indeed, Boyd, Korobkin and Moss⁽³⁾ have shown that when the noise from two commercial scanners are averaged and displayed as is done in our Fig. 3, the results are somewhat different than presented here. Aside from the choice of the filter used in the reconstruction algorithm, the noise present in the measured projection data may not be white.

3. The Detection Task

We wish to consider the effect that the unusual characteristics of CT noise might have upon the simple visual task of detecting the presence of circular objects in a CT image. The concept of signal-to-noise ratio (SNR) has been applied to this type of visual detection task by Rose,^(4,5) Schade⁽⁶⁾ and others⁽⁷⁾. The SNR for a circle of diameter d and contrast C present in a displayed image may be written as

$$\text{SNR} = \frac{C}{\sigma_d} \quad (12)$$

where σ_d is the r.m.s. deviation of the mean noise when averaged over a circular region of diameter d . It has been found experimentally that under optimum viewing condition human observers can detect squares in the presence of white noise with 50% certainty at a constant SNR value k over a large range of square sizes.⁽⁸⁾ The value of k ranges from 2 to 5.⁽⁷⁾ For squares whose angular subtense at the eye becomes greater than about 8 mrad the SNR threshold starts to increase with angular subtense. The required SNR also increases when the angular subtense falls below the sampling aperture of the eye, which is about 1 mrad under good lighting conditions.⁽⁷⁾ In the optimum operating region of the eye where the detection threshold SNR is a constant, we see that for white noise,

$$\text{SNR} = k = \frac{C_T \sqrt{A}}{\sigma} \quad (13)$$

where C_T is the threshold contrast at which the circle of Area A can be detected with some specific probability, and σ^2 is the noise variance per unit area (or pixel).

Figure 3 shows that for CT noise, $\sigma_d \sqrt{A}$ is not a constant, but, for large A , as A increases this product decreases potentially as fast as $A^{-1/4}$ or $d^{-1/2}$. If the human observer can detect the presence of circles at a constant SNR, as he can for white noise background, in the presence of CT noise we would expect that the quantity $\frac{C_T \sqrt{A}}{\sigma}$ would gradually decrease as \sqrt{A} increases beyond 3 or 4 pixels.

4. The Detectability Pattern

A detectability pattern has been developed which permits the testing of human observer response over a wide dynamic range of object sizes with relatively few images. The resulting detectability pattern is shown in Fig. 4. In this pattern the diameter of the circles increases by the factor $\sqrt{2}$ from 1 pixel diameter in the bottom row to 11.3 pixels diameter in the top row. For each column the product of the circle contrast times the circle diameter remains constant. This product increases by the factor $\sqrt{2}$ from one column to the next. The spacing between each row and column is 20 pixels. All circles are centered on a pixel. When white noise is superimposed upon this pattern, from Equation 13 it follows that the SNR remains constant for each column except for binning problems. The advantage of this pattern over the traditional Berger pattern⁽⁹⁾ is that the full range of circle diameters is maintained at each SNR for white noise. This pattern is also useful in demonstrating the general dependence of detectability upon circle diameter with a single image.

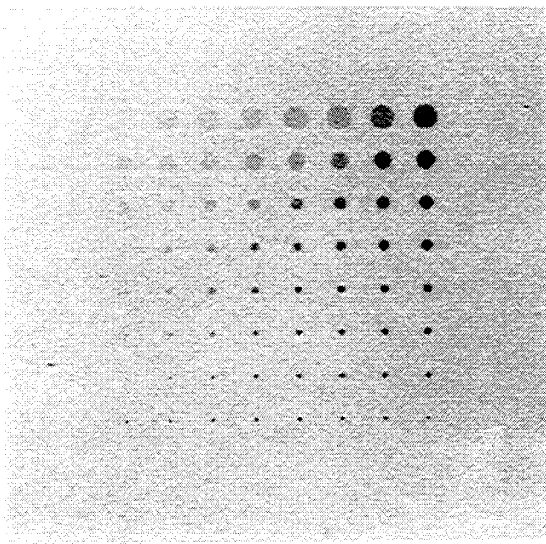


Figure 4

The detectability pattern. The diameter of the circles depicted start at one pixel width in the bottom row and increase by a factor of $\sqrt{2}$ from one row to the next. In each column the product of contrast times diameter remains constant. In going from one column to the next (to the left) this product decreases by $\sqrt{2}$.

DETECTABILITY IN THE PRESENCE OF COMPUTED TOMOGRAPHIC RECONSTRUCTION NOISE

5. Detectability Tests

Detectability tests were performed with the above described detectability pattern superimposed upon two types of noise, white and CT. In the white noise case, the pattern was simply binned in the 256 x 256 pixel display, i.e. the density in each pixel was proportional to the integral of the pattern over the area of that pixel. Thus, it is as if the pattern were reproduced with very high spatial resolution but subject to binning within the discrete pixel display. The white noise was generated by adding a Gaussian distributed random number to each pixel. For the CT noise pictures, CT reconstructions were computed from 300 projections taken of the detectability pattern to which white noise had been added. Thus, in the CT pictures the resolution of the test pattern was degraded by the finite sampling width of the projection and the reconstruction process. The pure ramp filter ($h = 1$) was used in the reconstruction. In order to determine what effect spatial averaging might have on detectability, the images were filtered using a Hanning filter of the form

$$H(f) = \begin{cases} \frac{1}{2} (1 + \cos 2\pi \frac{f}{f_N}), & f \leq \frac{f_N}{2} \\ 0 & , f > \frac{f_N}{2} \end{cases} \quad (14)$$

which is equal to 1/2 at $f_N/4$ and is zero beyond $f_N/2$. For the CT images this filtering was incorporated in the projection filter h whereas for the white noise images it was applied directly to the two dimensional image. The contrast of the filtered images was doubled over that of the unfiltered images. All test pictures were transferred from computer to 35 mm film using a video display unit. The 35 mm film image was printed on glossy photographic paper to a 10 cm x 10 cm size. Figures 5 and 6 show the unfiltered and filtered versions of the white and CT noise pictures used in these tests.

The human observers viewed the glossy prints from a distance of 30 to 40 cm under good lighting conditions. The angular subtense of 1 pixel was between 1.0 and 1.3 mrad. Thus the range of circle diameters 1 to 11.3 pixels, was mostly within the optimum operating region of the eye (Section 3), the largest circle being marginally larger than 8 mrad in subtense. The observers viewed one row of circles of the same diameter at a time. A mask was used to block out all but a strip of 25 pixels width. Numbers on the mask identified the columns of the pattern. The observer was asked to identify the last column in which he was "reasonably certain" he could see the circle. No attempt was made to correct for "false-positive" responses. Thus the results given here have a slightly ill-defined absolute normalization. However, they do provide a good relative measure of the threshold contrast between the various types of pictures used in the tests. It should be noted that since the position of the circle is known by the observer, the "problem of the search"⁽⁷⁾ is avoided here.

In the present series of detectability tests each type of picture was produced with 3 different noise levels superimposed upon the same detectability pattern. The r.m.s. noise levels were in the relationship 0.84:1:1.41. The noise patterns in the 3 images were varied by selecting different portions of the random number generator in order to average over random clumps of noise which might enhance or degrade a given circle. The reflective density in the background of the test pictures was maintained at about 0.4 density units. The r.m.s. density per pixel for the middle noise level was 0.13 and 0.046 for the unfiltered and filtered white noise pictures, respectively, and 0.19 and 0.040 for the unfiltered and filtered CT noise pictures. The tests were performed with 6 observers. Each observer was presented with 12 pictures (3 each of CT and white noise, both filtered and unfiltered). Thus, the threshold contrast for each circle diameter for each type of picture was determined from 18 observations. The internal consistency among the observers was found to be reasonably good: the r.m.s. deviation for the same circle diameter and same type of picture was 0.8 column numbers N , where $N \sim -2.9 \ln C_T \sqrt{A}$. If statistical averaging is performed, we might expect an error of $\sigma_N = 0.8/\sqrt{18} = 0.19$ or an error in $C_T \sqrt{A}$ of 6.8%.

It will be noted that the r.m.s. noise in the unfiltered CT images was about 1.5 times that in the unfiltered white noise image. There was some concern on the part of the author that at the rather large levels of noise present in the images, the detection response of the human observers might be non-linear. This would tend to bias the comparison between the response to CT noise and that to white noise. However, when the average detection thresholds for the high and low noise samples were compared, it was found that the ratio of $C_T \sqrt{A}$ for these two samples was 1.63 for white noise and 1.61 for CT noise. The ratio of the r.m.s. noise for these two samples was 1.68. Since $C_T \sqrt{A}$ scales with the r.m.s. noise we conclude that the noise levels used here are within the linear response region of the eye.

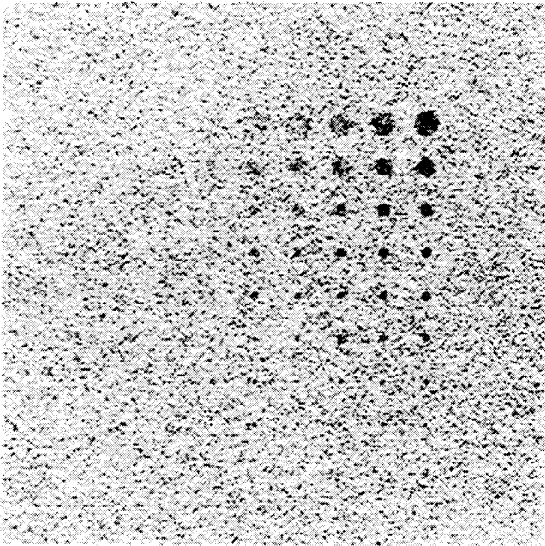


Figure 5a

White noise superimposed upon the detectability pattern of Figure 4.

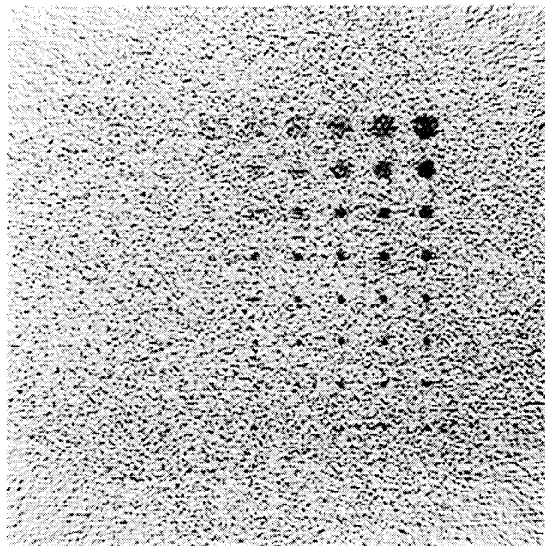


Figure 5b

A CT reconstruction of the pattern shown in Fig. 4 with white noise added to the projections. The rms noise in this figure is approximately the same as in Fig. 5a.

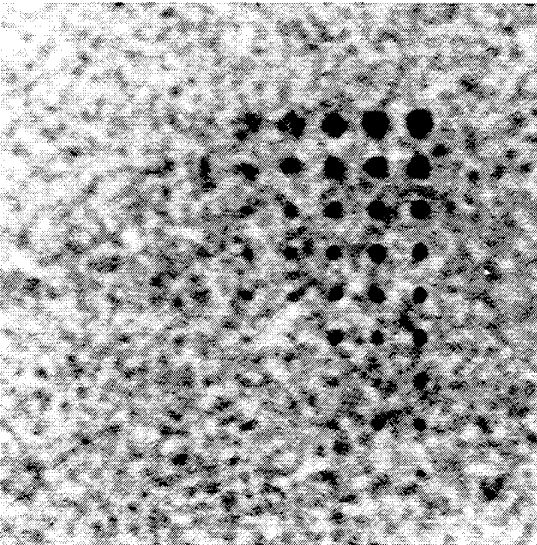


Figure 6a

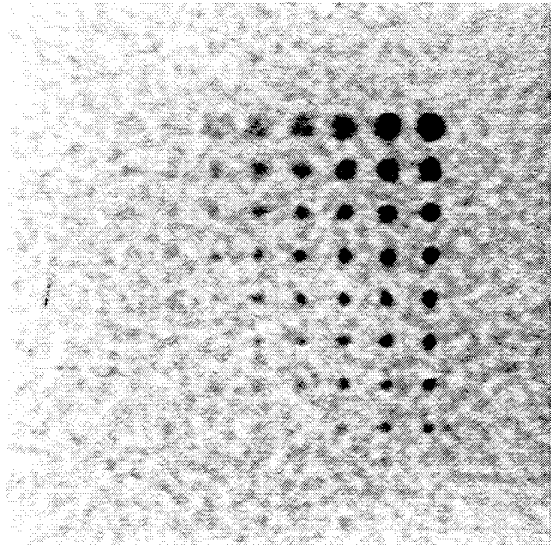


Figure 6b

Filtered versions of Figures 5a and b using a Hanning filter whose half value is at 1/4 the Nyquist frequency. The image contrast is increased by a factor of two.

6. Results

The results of the detectability tests described in the preceding section are summarized in Fig. 7. The ordinate variable is $(C_T\sqrt{A})/\sigma$, where C_T is the threshold contrast, A is the area of the circle (pixel^2) and σ is the r.m.s. noise in the unfiltered images. The same σ is used for the filtered images to allow a comparison of the threshold contrasts between the filtered and unfiltered images.

For unfiltered white noise the ordinate of Fig. 7 is the same as the SNR (Eq. 13) except for problems caused by the discrete binning into pixels. For example, a circle of 2 pixels

DETECTABILITY IN THE PRESENCE OF COMPUTED TOMOGRAPHIC RECONSTRUCTION NOISE

diameter centered on a pixel is spread out over 9 pixels in the display. The SNR depends upon the number of pixels included in the averaging. The optimum SNR occurs in this case for 5 pixels, the center pixels and the 4 nearest neighbors. For point plotted in Fig. 5, $(C_T\sqrt{A})/\sigma = 7.86$, the optimum SNR is in fact 5.6. When the unfiltered white noise results are expressed in terms of optimum SNR, it is found that the threshold SNR is constant at 5.5 to within 8% over the whole range of diameters. This is in agreement with earlier experiments summarized in Section 3. This discussion points to the need to have enough pixels within the area of the object to be detected to avoid discrete binning difficulties. Otherwise, the random placement of the object on the sampling array could lead to large fluctuations in the detection threshold. If the visual task involved the detection of small objects whose size was principally determined by the spatial resolution of the system, then it would be desirable to have at least 2 to 3 pixels within the width of the spatial resolution function.

The open circles in Fig. 7 show the effect on detectability when the white noise images are filtered as described in Section 5. The threshold contrast increases dramatically for the smaller circles since they are spread out over a larger area. The noise is reduced by the filtering but not as much as the signal. The net result is that the SNR drops for a given circle area which leads to a larger C_T required for detection. For circles with diameters greater than the FWHM of the resolution function, 4.7 pixels, the threshold contrast is essentially the same as for the unfiltered images. Thus the eye apparently can perform the spatial averaging of the white noise needed to detect these larger circles just as well as the computer.

For unfiltered CT noise the ordinate of Fig. 7 is not the same as the SNR. First, the method used to construct the CT images leads to a spatial resolution function which is broader than one pixel. This gives rise to the increase in $C_T\sqrt{A}$ as the circle diameter decreases below 3 pixels, just as in the case of the filtered white noise. Second, σ_d/\sqrt{A} is not a constant for CT noise but behaves as shown in Fig. 3. Figure 7 shows that $(C_T\sqrt{A})/\sigma$ levels off above 3 pixels diameter at a value comparable to that for the white noise. However, the threshold SNR in this region varies from 6.9 at 4 pixels diameter to 10.0 at 11.3 pixels, well above that required in the presence of white noise.

When the CT images are filtered (open squares in Fig. 7) a dramatic improvement is obtained for the detection of the larger circles. The average threshold contrast for 5.66 and 8 pixel diameters is decreased by a factor of 0.64. This is very close to the reduction of the r.m.s. CT noise over that of white noise, namely 0.59. It would appear from these data that the eye cannot perform the equivalent of algebraic averaging of CT noise as it can for white noise. Rather, it seems to process the noise as if it were white without taking advantage of the long-range negative correlations present in CT noise. When the averaging is done by the computer, the eye does much better in the detection of large circles. It is interesting to note that filtering the CT images increases detection capability even for the smaller diameter circles down to 2 pixels diameter, in contrast to what happens when white noise images are filtered. This is probably a result of the increased reduction in the r.m.s. noise for CT noise over that for white noise.

The results of the present study provoke a series of questions which can only be answered through further investigation. What would be

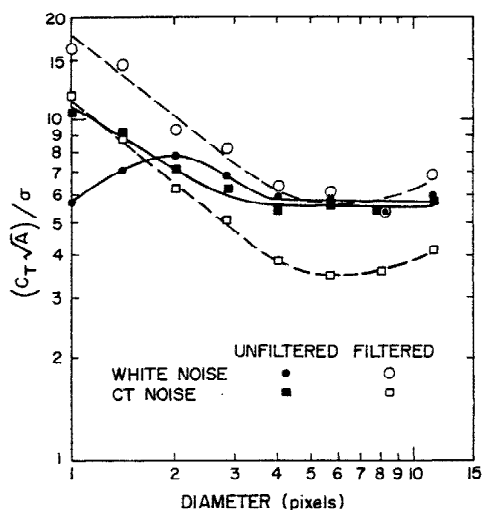


Figure 7

Summary of the observer detectability tests carried out using figures such as Fig. 5 and 6. C_T is the contrast of the circles at the threshold of detectability. A is the circle area and σ is the r.m.s. noise in the unfiltered images. It should be noted that the behavior of the unfiltered curves for diameters less than 3 pixels is strongly influenced by the detailed method of image formation as discussed in the text.

HANSON

present in commercial CT scanner images possess characteristics similar to those presented here for "ideal" CT noise?

7. Summary

The noise power spectrum of CT reconstruction noise has been derived. From this spectrum, the effect on the r.m.s. noise of spatial averaging or, equivalently, a CT image filtering is readily determined. The results of observer tests involving the detection of various sized circles indicates that spatial averaging substantially improves the detectability of large circles in the presence of CT noise. The implication is that the observer's eye cannot take into account the long-range negative correlations that exist in ideal CT noise. Further, in order to avoid large statistical fluctuations in the threshold contrast arising from the discrete binning of images into pixels, it is necessary to have at least 2 to 3 pixels within the width of the desired object (including spatial resolution).

Acknowledgments

I am indebted to T. Michael Cannon for the reconstruction and power estimation computer codes used here. The development of the detectability phantom was aided by conversations with Michael Goitein and Douglas Boyd. I have had many stimulating discussions with Robert Wagner on the subject of human detectability as well as with Stephen Riederer and David Chesler regarding noise power spectral properties of CT noise.

References

1. Riederer, S.J., Pelc, N.J. and Chesler, D.A., "Statistical Aspects of Computed X-Ray Tomography", presented at 4th International Conf. on Medical Physics, Ottawa, Canada, 1976 and submitted to Phys. Med. Bio.
2. Welch, P., IEEE Trans. Audio Electroacoust. AU-15, pp. 70-73. 1967.
3. Boyd, D.P., Korobkin, M.T. and Moss, A., SPIE Vol. 96, pp. 303-312. 1976.
4. Rose, A., J. Opt. Soc. Am. Vol. 38, pp. 196. 1948.
5. Rose, A., Vision: Human and Electronic, Plenum, New York 1973.
6. Schade, O.H., J. Soc. Motion Pict. Telev. Eng. Vol. 58, pp. 181. 1952.
7. Wagner, R.F., Med. Phys., Vol. 4, pp. 279-298. 1977.
8. Rosell, F.A. and Willson, R.H., in Perception of Displayed Information, Lucien M. Biberian, ed., Plenum Press New York 1973.
9. Burger, G.C.E., Philips Tech. Rev., Vol. 11, pp. 291. 1950.

Comment - Visual perception experiments using noise with power spectra similar to CT noise have been reported by M. J. Sakrison of the Electrical Engineering and Computer Science Department at Berkeley. Articles are published in Vision Research 1976 and 1977.

comment by - Art Burgess, University of B.C.

Response - I was unaware of Sakrison's work on this topic. Thank you for bringing his publications to my attention.

response by - Kenneth Hanson